Chapter 17

Other Beam Shapes

Overview: We have limited most of our discussion throughout the text up to this point to the lowest-order Gaussian-beam wave and its limiting forms leading to a plane wave or spherical wave. In this chapter we want to briefly examine other beam shapes that may have important propagation characteristics for certain applications. We first discuss *beam spreading* associated with higher-order *Hermite-Gaussian modes* and higher-order *Laguerre-Gaussian modes*. Our analysis of the *mean irradiance* is limited in each case to a particular lower-order mode. Next, we examine beam spreading and *scintillation* characteristics of an *annular beam*, also known as a "doughnut" beam.

We end this chapter with a brief introduction to other beam shapes such as the *flattened Gaussian* profile and the *Bessel beam*. Here, however, our treatment is limited to only free-space propagation characteristics.

17.1 Introduction

Most past studies of optical wave propagation have concentrated on infinite plane waves, spherical waves, or the lowest-order Gaussian-beam wave. By studying the lowest-order Gaussian-beam wave, it is easy to deduce results for the plane wave and spherical wave limits by simply specifying certain values of the Gaussian-beam parameters. However, there are other types of beams that are used in some applications, but their properties in atmospheric turbulence are not well known. These other beams include higher-order Hermite and Laguerre Gaussian beams, annular ("doughnut") beams, super Gaussian beams, flattened Gaussian profiles, and Bessel beams. In this short chapter we wish to examine a few of these other beam shapes to compare beam spreading and scintillation characteristics with those of a lowest-order Gaussian beam.

For reference purposes, we review the following definitions of beam parameters that characterize the basic Gaussian beam in either the plane of the transmitter or the plane of the receiver. If we start with a lowest-order TEM_{00} collimated Gaussian beam of radius W_0 in the plane of the transmitter, then after propagating a distance L to a receiver, the beam is characterized by the transmitter beam parameters

$$\Theta_0 = 1, \quad \Lambda_0 = \frac{2L}{kW_0^2}, \tag{1}$$

where k is the optical wave number. At the receiver, the corresponding parameters are

$$\Theta = 1 + \frac{L}{F}, \quad \Lambda = \frac{2L}{kW^2}, \tag{2}$$

where W and F denote the free-space spot radius and phase front radius of curvature in the plane of the receiver [see Chap. 4 for relations between (1) and (2)].

17.2 Beam Spreading: Higher-Order Gaussian Beams

Thus far we have primarily addressed the lowest-order Gaussian-beam wave, commonly called the TEM_{00} mode. However, in certain applications it may be advantageous to use other beams such as higher-order Gaussian beams, among other shapes. Some investigators have discussed the general propagation characteristics of these higher-order Gaussian beams in free space [1–4]. In particular, Carter [3] developed a definition for beam spot size of a Hermite-Gaussian beam of any order that reduces to known results for the TEM_{00} mode beam. Phillips and Andrews [4] followed that with a similar study for the Laguerre-Gaussian beam of any order. However, these particular studies are only for propagation through free space (see also Sections 4.7 and 4.8). In this section we wish to analyze beam spreading associated with some individual higher-order TEM_{mn} Gaussian beams in atmospheric turbulence for comparison with that of a lowest-order TEM_{00} Gaussian beam.

17.2.1 Hermite-Gaussian beam

In Chap. 4 we introduced the higher-order TEM_{mn} *Hermite-Gaussian beams* defined by

$$z = 0: \quad U_{mn}(x, y, 0) = H_m\left(\frac{\sqrt{2}x}{W_0}\right) H_n\left(\frac{\sqrt{2}y}{W_0}\right) \exp\left(-\frac{x^2}{W_0^2} - \frac{y^2}{W_0^2}\right), \tag{3}$$

where in the present analysis we assume the spot size along the x- and y-axes is the same, i.e., $W_{x,0} = W_{y,0} = W_0$. The functions $H_m(x)$ and $H_n(y)$ are Hermite polynomials. In discussing the free-space propagation of Hermite-Gaussian beams in Chap. 4, it was pointed out that the spot size of the pth mode in the receiver plane can be related to the irradiance by $I_{mn}(x, y, z)$ by

$$\sigma_{s,p}^2(z) = \frac{4 \int\int_{-\infty}^{\infty} s^2 I_{mn}(x, y, z) dx\, dy}{\int\int_{-\infty}^{\infty} I_{mn}(x, y, z) dx\, dy}, \tag{4}$$

where s represents either x or y and p denotes either m or n. Based on (4), therefore, the "effective spot size" in free space is given by the rectangular domain $\sigma_{xm}(z) \times \sigma_{yn}(z)$, where [3] ($W_x = W_y = W$)

$$\begin{aligned} \sigma_{x,m}(z) &= \sqrt{2m+1}W, \quad m = 0, 1, 2, \ldots, \\ \sigma_{y,n}(z) &= \sqrt{2n+1}W, \quad n = 0, 1, 2, \ldots, \end{aligned} \tag{5}$$

The parameter W has the same definition here as for the lowest-order Gaussian beam.

In this section we wish to investigate the spot size of such beams in the presence of optical turbulence. To begin, let us consider the special case of a Hermite-Gaussian TEM_{10} beam defined at the transmitter by

$$z = 0: \quad U_{10}(x, y, 0) = \left(\frac{2\sqrt{2}x}{W_0}\right) \exp\left(-\frac{x^2}{W_0^2} - \frac{y^2}{W_0^2}\right), \tag{6}$$

where the Hermite polynomial $H_1(x) = 2x$. The substitution of this expression into the Huygens-Fresnel integral yields the free-space optical field at some distance $z > 0$ [see Eq. (84) in Chap. 4]

$$\begin{aligned} U_{10}(x, y, z) = (\Theta - i\Lambda)&\left(\frac{\Theta - i\Lambda}{\Theta + i\Lambda}\right)^{3/2} \left(\frac{2\sqrt{2}x}{W}\right) \\ &\times \exp\left[\frac{ik}{2z}(\overline{\Theta} + i\Lambda)(x^2 + y^2)\right], \end{aligned} \tag{7}$$

where we have utilized the lowest-order Gaussian-beam parameters (2).

In the presence of atmospheric turbulence we use the *extended Huygens-Fresnel principle* [see Eq. (21) in Chap. 7] which, for the mean irradiance in rectangular

coordinates, leads to [5]

$$\begin{aligned}\langle I_{10}(x,y,z)\rangle = &\left(\frac{k}{2\pi z}\right)^2 \iiint\int_{-\infty}^{\infty} ds_{1x}ds_{1y}ds_{2x}ds_{2y}\left(\frac{2\sqrt{2}s_{1x}}{W_0}\right)\left(\frac{2\sqrt{2}s_{2x}}{W_0}\right)\\ &\times \exp\left[-\frac{1}{W_0^2}\left(1-\frac{i}{\Lambda_0}\right)s_{1x}^2-\frac{ik}{L}xs_{1x}\right]\exp\left[-\frac{1}{W_0^2}\left(1-\frac{i}{\Lambda_0}\right)s_{1y}^2-\frac{ik}{L}ys_{1y}\right]\\ &\times \exp\left[-\frac{1}{W_0^2}\left(1+\frac{i}{\Lambda_0}\right)s_{2x}^2+\frac{ik}{L}xs_{2x}\right]\exp\left[-\frac{1}{W_0^2}\left(1+\frac{i}{\Lambda_0}\right)s_{2y}^2+\frac{ik}{L}ys_{2y}\right]\\ &\times \exp\left[-\frac{1.78\sigma_1^2}{2\Lambda_0 W_0^2}\left(s_{1x}^2+s_{1y}^2+s_{2x}^2+s_{2y}^2-2s_{1x}s_{2x}-2s_{1y}s_{2y}\right)\right],\end{aligned} \tag{8}$$

where we have defined $\mathbf{s}_1 = \langle s_{1x}, s_{1y}\rangle$, $\mathbf{s}_2 = \langle s_{2x}, s_{2y}\rangle$. The argument of the last exponential function in (8) is deduced from the spherical wave structure function based on the Kolmogorov spectrum and a quadratic approximation, i.e.,

$$\begin{aligned}D_{\rm sp}(|\mathbf{s}_1-\mathbf{s}_2|,z) &= 1.09C_n^2k^2z|\mathbf{s}_1-\mathbf{s}_2|^{5/3}\\ &\cong \frac{1.78\sigma_R^2}{\Lambda_0 W_0^2}|\mathbf{s}_1-\mathbf{s}_2|^2,\end{aligned} \tag{9}$$

where $\sigma_R^2 = 1.23C_n^2k^{7/6}z^{11/6}$ is the *Rytov variance*. The subsequent evaluation of (8) yields

$$\begin{aligned}\langle I_{10}(x,y,z)\rangle = &\left[\frac{8x^2W_0^2}{W^4\left(1+1.78\Lambda\sigma_R^2\right)^3}+\frac{3.56\Lambda\sigma_R^2\left(1+\Lambda\sigma_R^2\right)}{\left(1+1.78\Lambda\sigma_R^2\right)^3}\right]\\ &\times\exp\left[-\frac{2(x^2+y^2)}{W^2\left(1+1.78\Lambda\sigma_R^2\right)}\right],\end{aligned} \tag{10}$$

or, on splitting (10) into x and y components, we observe that

$$\begin{aligned}\langle I_{10}(x,y,z)\rangle_x = &\frac{W_0}{W\sqrt{1+1.78\Lambda\sigma_R^2}}\left[\frac{8x^2}{W^2\left(1+1.78\Lambda\sigma_R^2\right)^2}+\frac{3.56\Lambda_0\sigma_R^2\left(1+\Lambda\sigma_R^2\right)}{\left(1+1.78\Lambda\sigma_R^2\right)^2}\right]\\ &\times\exp\left[-\frac{2x^2}{W^2\left(1+1.78\Lambda\sigma_R^2\right)}\right],\end{aligned} \tag{11}$$

$$\langle I_{10}(x,y,z)\rangle_y = \frac{W_0}{W\sqrt{1+1.78\Lambda\sigma_R^2}}\exp\left[-\frac{2y^2}{W^2(1+1.78\Lambda\sigma_R^2)}\right]. \tag{12}$$

In the limit $\sigma_{\rm R}^2 = 0$, Eq. (10) reduces to the free-space result

$$I_{10}(x,y,z) = \frac{8x^2W_0^2}{W^4}\exp\left[-\frac{2\left(x^2+y^2\right)}{W^2}\right]. \tag{13}$$

In Fig. 17.1 we plot the normalized mean irradiance (10) as a function of x and $y = 0$ corresponding to the cases: free space, moderate turbulence, and strong turbulence. The normalization is obtained by scaling the mean irradiance (10)

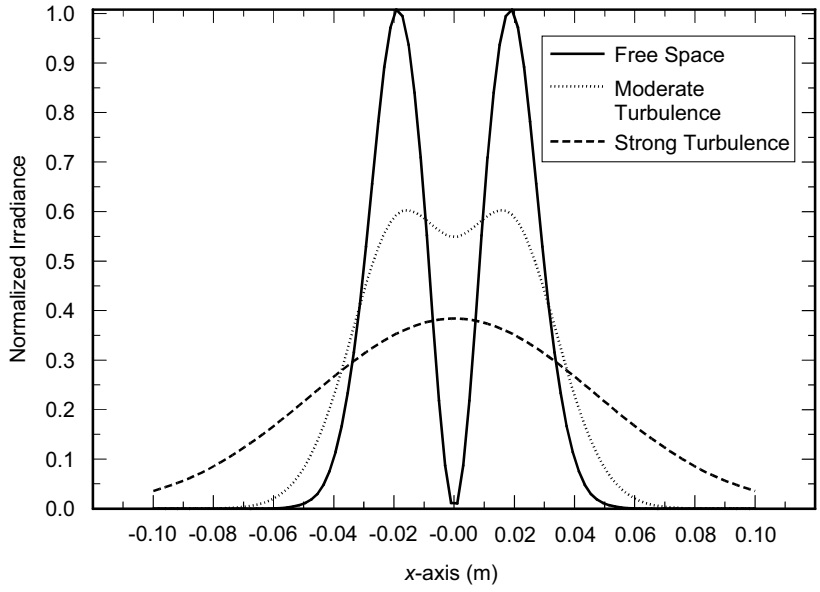

Figure 17.1 Irradiance of a TEM_{10} Hermite-Gaussian beam scaled by the maximum irradiance in free space as a function of radial distance from the optical axis and various levels of atmospheric turbulence.

by the maximum value in free space obtained from (13). Here we see that in strong turbulence the mean irradiance profile resembles that of a lowest-order Gaussian-beam wave.

Based on the spot size definition (4) using the mean irradiance, the substitution of (11) and (12) into (4) leads to the beam width along the x-axis and y-axis, respectively, of a TEM_{10} Hermite-Gaussian beam given by

$$\sigma_{x,1,\mathrm{LT}} = W\sqrt{1+1.78\Lambda\sigma_R^2}\sqrt{\frac{3\left(1+1.78\Lambda\sigma_R^2\right)+1.78\Lambda_0\sigma_R^2\left(1+\Lambda\sigma_R^2\right)}{1+1.78\Lambda\sigma_R^2+1.78\Lambda_0\sigma_R^2\left(1+\Lambda\sigma_R^2\right)}}, \tag{14}$$

$$\sigma_{y,0,\mathrm{LT}} = W\sqrt{1+1.78\Lambda\sigma_R^2}. \tag{15}$$

Note that (14) reduces properly to $\sigma_{x,1} = \sqrt{3}W$ in the limit of free-space propagation.

To make a comparison of the spreading of the TEM_{10} Hermite-Gaussian beam with the TEM_{00} Gaussian beam having the same spot size at the transmitter, we examine the ratios $\sigma_{x,1}/\sigma_{x,1\mathrm{LT}}$ and W/W_{LT} in Fig. 17.2. Note that the higher-order TEM_{10} mode experiences less additional beam spreading beyond diffraction than the lowest-order TEM_{00} Gaussian beam.

Although the mean irradiance for the general Hermite-Gaussian beam has not yet been developed in closed form, Shirai et al. [6] did derive closed-form expressions for the spot size of the beam, based on Eq. (4) and a quadratic approximation for the spherical-wave structure function. However, in their analysis, they

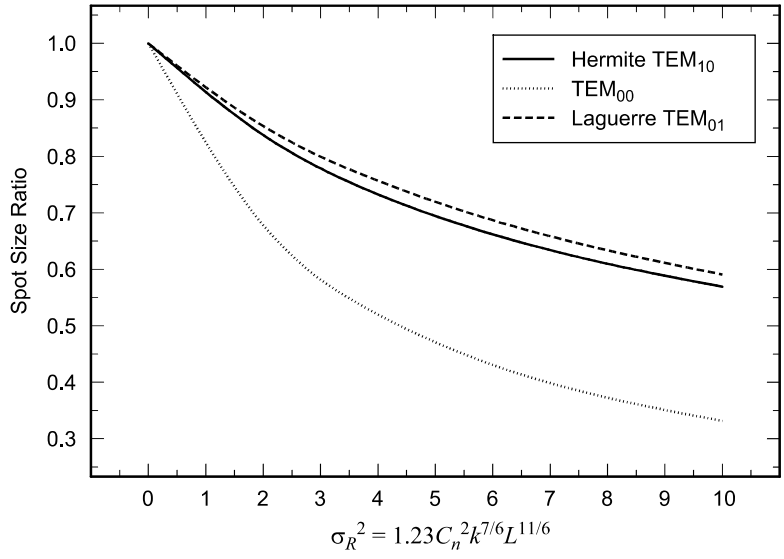

Figure 17.2 Ratio of spot size in free space to spot size in turbulence.

used the approximation

$$J_0(\kappa\xi\rho) \cong 1 - \frac{1}{4}(\kappa\xi\rho)^2, \quad \kappa\xi\rho \ll 1, \tag{16}$$

and found the expressions

$$\sigma_{x,m,\mathrm{LT}} = \sqrt{(2m+1)W^2 + \frac{8}{3}\pi^2 z^3 \int_0^\infty \kappa^3 \Phi_n(\kappa) d\kappa}, \tag{17}$$

$$\sigma_{y,n,\mathrm{LT}} = \sqrt{(2n+1)W^2 + \frac{8}{3}\pi^2 z^3 \int_0^\infty \kappa^3 \Phi_n(\kappa) d\kappa}. \tag{18}$$

The integral term in (17) and (18) is related to T defined by (38) in Chap. 6 under a geometrical optics approximation. Shirai et al. also concluded that the relative spreading of all order Hermite-Gaussian modes is smaller than that of the lower-order modes, in particular, the TEM_{00} case.

17.2.2 Laguerre-Gaussian beam

The notion of a higher-order *Laguerre-Gaussian beam* was also briefly introduced in Chap. 4. These higher-order modes are defined in the plane of the transmitter by the cylindrical coordinate representation (r, θ, z)

$$z = 0: \quad U_{mn}(r,\theta,0) = \left(\frac{\sqrt{2}r}{W_0}\right)^m (-i^m) \exp(im\theta) \exp\left(\frac{-r^2}{W_0^2}\right) L_n^{(m)}\left(\frac{2r^2}{W_0^2}\right), \tag{19}$$

where $\mathbf{r}$ is a vector in the transverse plane at angle θ, $r = |\mathbf{r}|$, W_0 is the radius of the TEM_{00} mode beam, $L_n^{(m)}(x)$ is the *associated Laguerre polynomial*, and n and m are the radial and angular mode numbers. Similar to the Hermite-Gaussian beam case, the spot size of a Laguerre-Gaussian beam can be defined by

$$\sigma_{mn}^2(z) = \frac{2\int_0^{2\pi}\int_0^{\infty} r^2 I_{mn}(r,\theta,z) r dr\, d\theta}{\int_0^{2\pi}\int_0^{\infty} I_{mn}(r,\theta,z) r dr\, d\theta}. \tag{20}$$

From this last expression we can readily obtain the free-space result [4]

$$\sigma_{mn}(z) = \sqrt{2n+m+1}W; \qquad m,n = 0,1,2,\ldots. \tag{21}$$

To calculate the spot size in optical turbulence, we limit our treatment to the special case in which and $m = 0$ and $n = 1$. First, recall that the free-space irradiance for this beam at distance z from the transmitter is (see Section 4.7.4)

$$I(r,\theta,z)_{01} = \frac{W_0^2}{W^2}\left(1 - \frac{2r^2}{W^2}\right)\exp\left(-\frac{2r^2}{W^2}\right), \tag{22}$$

where we have written $L_1^{(0)}(x) = 1 - x$. Based on (21), the free-space spot size for this beam is $\sigma_{01}(z) = \sqrt{3}W$. In the presence of optical turbulence, we once again use the extended Huygens-Fresnel integral and the quadratic approximation for the spherical wave structure function given by (9). The calculation this time leads to the form of the mean irradiance in the plane of the receiver given by [5]

$$\langle I_{01}(r,\theta,z)\rangle = \left(A + \frac{Br^2}{W^2} + \frac{Cr^4}{W^4}\right)\exp\left[-\frac{2r^2}{W^2(1+1.78\Lambda\sigma_R^2)}\right], \tag{23}$$

where

$$A = \frac{\Theta^2\left(1+0.79\sigma_R^4\right) - \Lambda^2}{\left(1+1.78\Lambda\sigma_R^2+0.79\Theta\sigma_R^4\right)\left(1+1.78\Lambda\sigma_R^2\right)} + \frac{2\Lambda^2 - 1.78\Lambda\Theta\sigma_R^2}{\left(1+1.78\Lambda\sigma_R^2\right)^2}$$
$$- \frac{0.79\sigma_R^4\left(2\Lambda^2\Theta + 1.78\Lambda\Theta^2\sigma_R^2\right)}{\left(1+1.78\Lambda\sigma_R^2+0.79\Theta\sigma_R^4\right)\left(1+1.78\Lambda\sigma_R^2\right)^2} + \frac{6.34\Lambda^2\Theta\sigma_R^4}{\left(1+1.78\Lambda\sigma_R^2\right)^3}, \tag{24}$$

$$B = -\frac{4\Theta\left(1-1.78\Lambda\sigma_R^2\right)}{\left(1+1.78\Lambda\sigma_R^2\right)^4}, \quad C = \frac{4\Theta}{\left(1+1.78\Lambda\sigma_R^2\right)^5}. \tag{25}$$

In Fig. 17.3 we plot the normalized mean irradiance (23) as a function of r corresponding to the cases: free space, moderate turbulence, and strong turbulence. The normalization is obtained by scaling the mean irradiance (23) by its maximum value in free space, viz., W_0^2/W^2. Once again we see that in strong turbulence the mean irradiance profile resembles that of a lowest-order Gaussian-beam wave.

In calculating the predicted spot radius of the Laguerre-Gaussian beam, we substitute (23) into (20) to obtain

$$\sigma_{01,\mathrm{LT}} = W\sqrt{3 + 1.78\Lambda\sigma_R^2}. \tag{26}$$

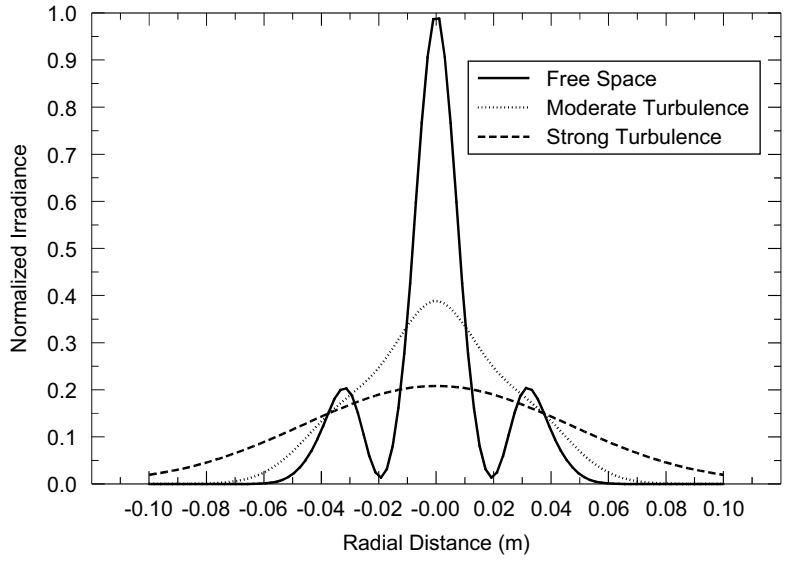

Figure 17.3 Irradiance of a TEM_{01} Laguerre-Gaussian beam scaled by the maximum irradiance in free space as a function of radial distance from the optical axis and various levels of atmospheric turbulence.

Note that (26) is somewhat simpler than the corresponding expression (13) for a Hermite-Gaussian beam. Also, in the absence of turbulence (26) reduces to the free-space spot size given by (21). In Fig. 17.2 we show a comparison of beam spreading of the TEM_{01} Laguerre-Gaussian beam with the TEM_{00} Gaussian beam and the TEM_{10} Hermite-Gaussian beam, plotting the ratios $\sigma_{01}/\sigma_{01,\text{LT}}$ and W/W_{LT}. The predicted beam spreading of the Laguerre-Gaussian beam is nearly the same as that of the Hermite-Gaussian beam, but both show less beam spreading than the TEM_{00} beam, particularly under stronger fluctuations ($\sigma_R^2 > 1$).

Like that shown in the case of higher-order Hermite-Gaussian beams, it is anticipated that individual higher-order Laguerre-Gaussian beams will also experience less additional broadening (on a percentage basis) due to turbulence than experienced by the lower-order Gaussian beam modes. That is, because the higher-order mode structure places more energy of the beam away from the beam axis, the incremental spreading due to turbulence should be less. This reduced spreading in the higher-order modes may have important benefits in various applications, such as free-space laser communications, where power losses caused by atmospheric turbulence reduce the performance level of the system.

17.3 Annular Beam

Laser beams with shapes other than the lowest-order TEM_{00} Gaussian beam can have favorable beam broadening and scintillation characteristics over the Gaussian beam. In particular, we observed in Section 17.2 that higher-order Hermite-Gaussian

or Laguerre-Gaussian beams show less beam spreading than the lowest-order Gaussian beam. In this section we wish to perform a similar analysis on a laser beam with an annular (doughnut-shape) cross section at the transmitter. For obvious reasons, we refer to this as an *annular beam.* Annular beams can be generated in several ways. For example, a ring-shaped laser beam (annular beam) is created when a TEM_{00} Gaussian laser beam is propagated through an annular aperture, and such apertures exist in many telescopes with a secondary mirror (obscuration). Also, high-power lasers use unstable optical resonators as resonant cavities and these produce an annular output beam.

It has been known for a long time that the free-space Fraunhofer pattern of an annular beam shows an on-axis peak in its far-field irradiance distribution [7], indicating that the hole in the beam at the transmitter has filled through the propagation process. This has the effect of redistributing the power. The same general behavior has also been predicted in the presence of atmospheric turbulence [8].

17.3.1 Free-space irradiance

We model the annular beam as the difference of two Gaussian beams called *beam A* and *beam B.* Doing so permits us to utilize some of the theory developed for Gaussian beam waves in our analysis. Hence, at the transmitter we write

$$z = 0: \quad U_0(\mathbf{r}, 0) = U_{A,0}(\mathbf{r}, 0) - U_{B,0}(\mathbf{r}, 0), \tag{27}$$

where the two fields on the right-hand side are unit-amplitude Gaussian beams, i.e.,

$$U_{A,0}(\mathbf{r}, 0) = \exp\left(-\frac{r^2}{W_{A,0}^2} - \frac{ikr^2}{2F_{A,0}}\right), \quad U_{B,0}(\mathbf{r}, 0) = \exp\left(-\frac{r^2}{W_{B,0}^2} - \frac{ikr^2}{2F_{B,0}}\right). \tag{28}$$

Here, $W_{A,0}$, $W_{B,0}$ are the beam radii and $F_{A,0}$, $F_{B,0}$ are the phase front radii of curvature. For our analysis we take the case of two collimated beams in which $F_{A,0} = F_{B,0} = \infty$. Also, we impose the restriction on beam radii $W_{A0} > W_{B0}$.

Because the field (27) is a sum of field terms, the Huygens-Fresnel integral leads to the field representation at distance L from the transmitter given by

$$z = L: \quad U_0(\mathbf{r}, L) = U_{A,0}(\mathbf{r}, L) - U_{B,0}(\mathbf{r}, L), \tag{29}$$

where

$$\begin{aligned} U_{A,0}(\mathbf{r}, L) &= \frac{W_{A,0}}{W_A}\exp\left(ikL - i\varphi_A - \frac{r^2}{W_A^2} - \frac{ikr^2}{2F_A}\right), \\ U_{B,0}(\mathbf{r}, 0) &= \frac{W_{B,0}}{W_B}\exp\left(ikL - i\varphi_B - \frac{r^2}{W_B^2} - \frac{ikr^2}{2F_B}\right). \end{aligned} \tag{30}$$

The definitions of spot radius, longitudinal phase, and phase front radius of curvature for each beam in (29) follows that introduced for a single beam, except here we subscript all parameters with either A or B including the nondimensional

Gaussian beam parameters

$$\begin{aligned}
&\Theta_{A,0} = 1, \quad \Lambda_{A,0} = \frac{2L}{kW_{A,0}^2}; \quad \Theta_A = \frac{\Theta_{A,0}}{\Theta_{A,0}^2 + \Lambda_{A,0}^2}, \quad \Lambda_A = \frac{\Lambda_{A,0}}{\Theta_{A,0}^2 + \Lambda_{A,0}^2}, \\
&\Theta_{B,0} = 1, \quad \Lambda_{B,0} = \frac{2L}{kW_{B,0}^2}; \quad \Theta_B = \frac{\Theta_{B,0}}{\Theta_{B,0}^2 + \Lambda_{B,0}^2}, \quad \Lambda_B = \frac{\Lambda_{B,0}}{\Theta_{B,0}^2 + \Lambda_{B,0}^2}.
\end{aligned} \tag{31}$$

The *free-space irradiance* deduced from (29) takes the form

$$\begin{aligned}
I^0(\mathbf{r}, L) &= U_{A,0}(\mathbf{r}, L)U_{A,0}^*(\mathbf{r}, L) + U_{B,0}(\mathbf{r}, L)U_{B,0}^*(\mathbf{r}, L) \\
&\quad - U_{A,0}(\mathbf{r}, L)U_{B,0}^*(\mathbf{r}, L) - U_{B,0}(\mathbf{r}, L)U_{A,0}^*(\mathbf{r}, L) \\
&= I_{A,0}(\mathbf{r}, L) + I_{B,0}(\mathbf{r}, L) - 2\sqrt{I_{A,0}(\mathbf{r}, L)I_{B,0}(\mathbf{r}, L)}\cos(\Delta\varphi + r^2\Delta F),
\end{aligned} \tag{32}$$

where $I_{A,0}(\mathbf{r}, L)$ and $I_{B,0}(\mathbf{r}, L)$ are the free-space irradiances of beam A and beam B, respectively. The last term in (32) is the cross-term, arising from the interaction between the two optical fields, where

$$\Delta\varphi = \varphi_A - \varphi_B, \quad \Delta F = \frac{k}{2}\left(\frac{1}{F_A} - \frac{1}{F_B}\right). \tag{33}$$

Here, the quantities φ_A and φ_B refer to longitudinal phase terms at the receiver.

We illustrate the free-space irradiance (32) in Fig. 17.4 as a function of propagation distance z and distance r off the optical axis. We have scaled the irradiance by the on-axis irradiance of beam A given by $I_{A,0}(0, L)$. The outer radius of the annular beam at the transmitter is 2 cm, the inner radius is 1.8 cm, and the wavelength is 1.55 μm. Note that the hole in the middle of the annular beam at the transmitter is filled in and replaced by a temporary peak in the on-axis irradiance as the beam propagates in free space. Eventually, diffraction effects cause the beam to spread and the on-axis peak disappears. In this case the irradiance of the annular beam resembles that of a single Gaussian-beam wave.

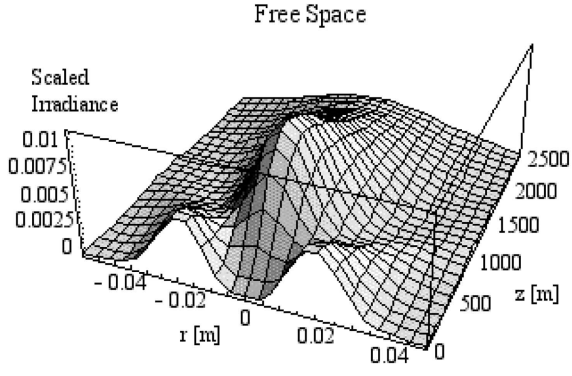

Figure 17.4 The free-space irradiance distribution of an annular beam scaled by the on-axis irradiance of beam *A*.

17.3.2 Mean irradiance in atmospheric turbulence

The mean irradiance can theoretically be determined by either the Rytov approximation or by the extended Huygens-Fresnel principle. Once again, we choose the latter. In using this method, the aperture distribution is separated from the propagation problem because the effect of optical turbulence is based on a spherical wave.

In the case of the annular beam, the mean irradiance consists of four terms,

$$\langle I(r,L)\rangle = \langle I_{AA}(r,L)\rangle + \langle I_{BB}(r,L)\rangle - \langle I_{AB}(r,L)\rangle - \langle I_{BA}(r,L)\rangle, \tag{34}$$

where the first two terms on the right-hand side represent the mean irradiance of Gaussian beams A and B, respectively. Therefore, we have

$$\begin{aligned}\langle I_{AA}(r,L)\rangle &= \langle U_A(r,L)U_A^*(r,L)\rangle \\ &= \left(\frac{k}{2\pi L}\right)^2 \int\int\int\int_{-\infty}^{\infty} d^2s_1 d^2s_2 U_{A,0}(\mathbf{s}_1,0)U_{A,0}^*(\mathbf{s}_2,0) \\ &\quad \times \exp\left[\frac{ik}{2L}\left(|\mathbf{s}_1-\mathbf{r}|^2 - |\mathbf{s}_2-\mathbf{r}|^2\right)\right]\exp\left[-\frac{1}{2}D_{\rm sp}(|\mathbf{s}_1-\mathbf{s}_2|)\right] \\ &= \frac{W_{A,0}^2}{W_{A,\rm LT}^2}\exp\left(-\frac{2r^2}{W_{A,\rm LT}^2}\right),\end{aligned} \tag{35}$$

and similarly,

$$\langle I_{BB}(r,L)\rangle = \langle U_B(r,L)U_B^*(r,L)\rangle = \frac{W_{B,0}^2}{W_{B,\rm LT}^2}\exp\left(-\frac{2r^2}{W_{B,\rm LT}^2}\right), \tag{36}$$

where the long-term spot radii are defined by

$$\begin{aligned}W_{A,\rm LT} &= W_{A,0}\sqrt{\Theta_{A,0}^2+\Lambda_{A,0}^2}\sqrt{1+0.98\sigma_R^2 Q_m^{1/6}\Lambda_A}, \\ W_{B,\rm LT} &= W_{B,0}\sqrt{\Theta_{B,0}^2+\Lambda_{B,0}^2}\sqrt{1+0.98\sigma_R^2 Q_m^{1/6}\Lambda_B}\end{aligned} \tag{37}$$

In Eqs. (36) the parameter $Q_m = L\kappa_m^2/k = 35.05L/kl_0^2$, where l_0 is the inner scale of turbulence. In arriving at the results of (35) and (36) we used the spherical wave structure function in the form (see also Section 7.3.3) $D_{\rm sp}(\rho) = 1.09C_n^2k^2Ll_0^{-1/3}\rho^2$. The remaining cross-terms in (34) are defined by

$$\begin{aligned}\langle I_{AB}(r,L)\rangle &= \langle I_{BA}^*(r,L)\rangle \\ &= \left(\frac{k}{2\pi L}\right)^2 \int\int_{\infty}^{\infty} d^2S \int\int_{-\infty}^{\infty} d^2Q \exp\left[-\left(S^2+\frac{1}{4}Q^2\right)\left(\frac{1}{W_{A,0}^2}+\frac{1}{W_{B,0}^2}\right)\right] \\ &\quad \times \exp\left\{\left[\frac{ik}{L}-\left(\frac{1}{W_{A,0}^2}+\frac{1}{W_{B,0}^2}\right)\right]\mathbf{S}\cdot\mathbf{Q}\right\}\exp\left(-\frac{ik}{L}\mathbf{Q}\cdot\mathbf{r}\right)\exp\left[-\frac{1}{2}D_{\rm sp}(Q)\right],\end{aligned} \tag{38}$$

where we have introduced the vectors $\mathbf{S} = \left(\frac{1}{2}\right)(\mathbf{s}_1+\mathbf{s}_2), \mathbf{Q} = \mathbf{s}_1-\mathbf{s}_2$.

The evaluation of three of the above integrals yields

$$\begin{aligned}\langle I_{AB}(r,L)\rangle &= \langle I_{BA}^{*}(r,L)\rangle \\ &= \left(\frac{k}{2L}\right)^{2}\frac{W_{A,0}^{2}W_{B,0}^{2}}{\left(W_{A,0}^{2}+W_{B,0}^{2}\right)}\int_{0}^{\infty}QJ_{0}\left(\frac{krQ}{L}\right)\exp\left[-\frac{1}{2}D_{\mathrm{ap}}(Q)\right] \\ &\quad\times\exp\left\{-\left[\frac{1+\left(k/2L^{2}\right)W_{A,0}^{2}W_{B,0}^{2}}{W_{A,0}^{2}+W_{B,0}^{2}}-\frac{ik}{2L}\frac{\left(W_{A,0}^{2}-W_{B,0}^{2}\right)}{W_{A,0}^{2}+W_{B,0}^{2}}\right]Q^{2}\right\}dQ,\end{aligned} \tag{39}$$

which reduces to

$$\begin{aligned}\langle I_{AB}(r,L)\rangle = \langle I_{BA}^{*}(r,L)\rangle &= \left(\frac{k}{2L}\right)^{2}\frac{W_{A,0}^{2}W_{B,0}^{2}}{\sqrt{u^{2}+v^{2}}}\exp\left[-\frac{\left(W_{A,0}^{2}+W_{B,0}^{2}\right)k^{2}r^{2}u}{4L^{2}\sqrt{u^{2}+v^{2}}}\right] \\ &\quad\times\exp\left[i\tan^{-1}\left(\frac{v}{u}\right)-\frac{i\left(W_{A,0}^{2}+W_{B,0}^{2}\right)k^{2}r^{2}u}{4L^{2}\sqrt{u^{2}+v^{2}}}\right].\end{aligned} \tag{40}$$

For mathematical simplicity in (41) we have introduced the quantities

$$\begin{aligned}u &= 1+\left(\frac{k}{2L}\right)^{2}W_{A,0}^{2}W_{B,0}^{2}+0.55C_{n}^{2}k^{2}Ll_{0}^{-1/3}\left(W_{A,0}^{2}+W_{B,0}^{2}\right), \\ v &= \frac{k}{2L}\left(W_{A,0}^{2}-W_{B,0}^{2}\right).\end{aligned} \tag{42}$$

Last, by combining (35), (36), and (41), we obtain the mean irradiance for the annular beam given by

$$\begin{aligned}\langle I(r,L)\rangle &= \frac{W_{A,0}^{2}}{W_{A,\mathrm{LT}}^{2}}\exp\left(-\frac{2r^{2}}{W_{A,\mathrm{LT}}^{2}}\right)+\frac{W_{B,0}^{2}}{W_{B,\mathrm{LT}}^{2}}\exp\left(-\frac{2r^{2}}{W_{B,\mathrm{LT}}}\right) \\ &\quad-2\left(\frac{k}{2L}\right)^{2}\frac{W_{A,0}^{2}W_{B,0}^{2}}{\sqrt{u^{2}+v^{2}}}\exp\left[-\frac{\left(W_{A,0}^{2}+W_{B,0}^{2}\right)k^{2}r^{2}u}{4L^{2}\sqrt{u^{2}+v^{2}}}\right] \\ &\quad\times\cos\left[\tan^{-1}\left(\frac{v}{u}\right)-\frac{\left(W_{A,0}^{2}+W_{B,0}^{2}\right)k^{2}r^{2}u}{4L^{2}\sqrt{u^{2}+v^{2}}}\right].\end{aligned} \tag{42}$$

The mean irradiance profile (43) is displayed in Fig. 17.5 as a function of propagation distance and transverse radial distance for two different values of the refractive-index structure constant C_n^2. The value $C_n^2 = 10^{-12}\ \mathrm{m}^{-2/3}$ corresponds to very strong optical turbulence conditions whereas the value $C_n^2 = 10^{-14}\ \mathrm{m}^{-2/3}$ is much weaker and perhaps more typical. The inner scale in both cases was set at $l_0 = 1$ mm. We have chosen the same beam characteristics in Fig. 17.5 as that shown in Fig. 17.4, viz., beam radii of 1.8 and 2 cm, and wavelength 1.55 μm. In Fig. 17.6 we plot the same beam at various distances from the transmitter but this time with refractive-index values $C_n^2 = 10^{-13}\ \mathrm{m}^{-2/3}$ and $C_n^2 = 10^{-12}\ \mathrm{m}^{-2/3}$. Also shown for comparison is the irradiance profile of the beam in free space. As in

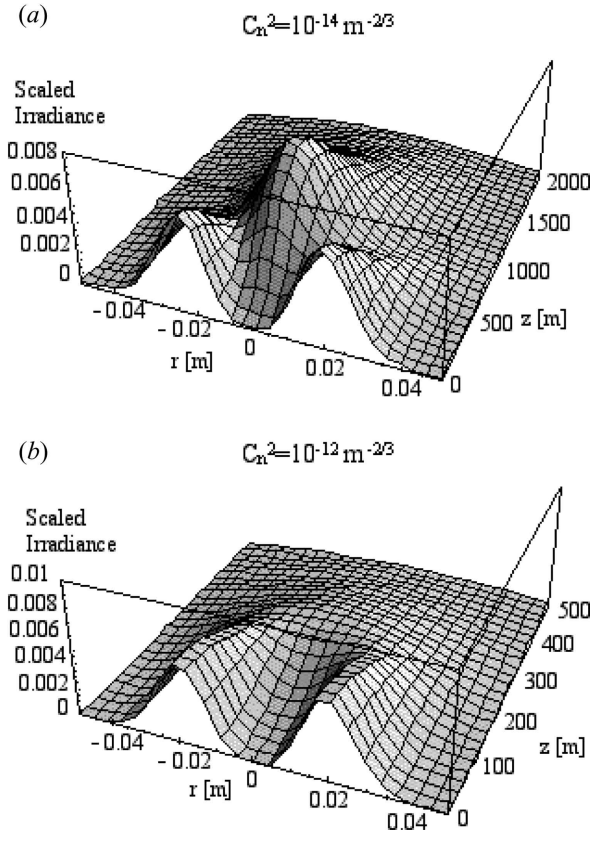

Figure 17.5 The mean irradiance of the annular beam scaled by $I_A(0,0)$ for cases (a) $C_n^2 = 10^{-14}\mathrm{m}^{-2/3}$, $l_0 = 1$ mm and (b) $C_n^2 = 10^{-12}\,\mathrm{m}^{-2/3}$, $l_0 = 1$ mm. In both cases the beam radii are 1.8 and 2 cm and the wavelength is $\lambda = 1.55$ μm.

Fig. 17.5, we see that in the presence of strong optical turbulence ($C_n^2 = 10^{-12}\,\mathrm{m}^{-2/3}$) the profile of the beam is quite distinct from that in weaker turbulence or in free space.

17.3.3 Scintillation

In this section we develop expressions for the scintillation index of an annular beam using the Rytov approximation. To do so, we must develop new spectral representations for the complex phase perturbation $\psi_1(\mathbf{r}, L)$ to account for the change in beam profile.

We begin by recalling the spectral representation for the first-order complex phase perturbation given by [see Eq. (36) in Chap. 5]

$$\psi(\mathbf{r}, L) = \frac{k^2}{2\pi}\int_0^L dz \int\int_{-\infty}^{\infty} d^2s \exp\left[ik(L-z) + \frac{ik|\mathbf{s}-\mathbf{r}|^2}{2(L-z)}\right]\frac{U_0(\mathbf{s}, z)}{U_0(\mathbf{r}, L)}\frac{n_1(\mathbf{s}, z)}{(L-z)}. \quad (43)$$

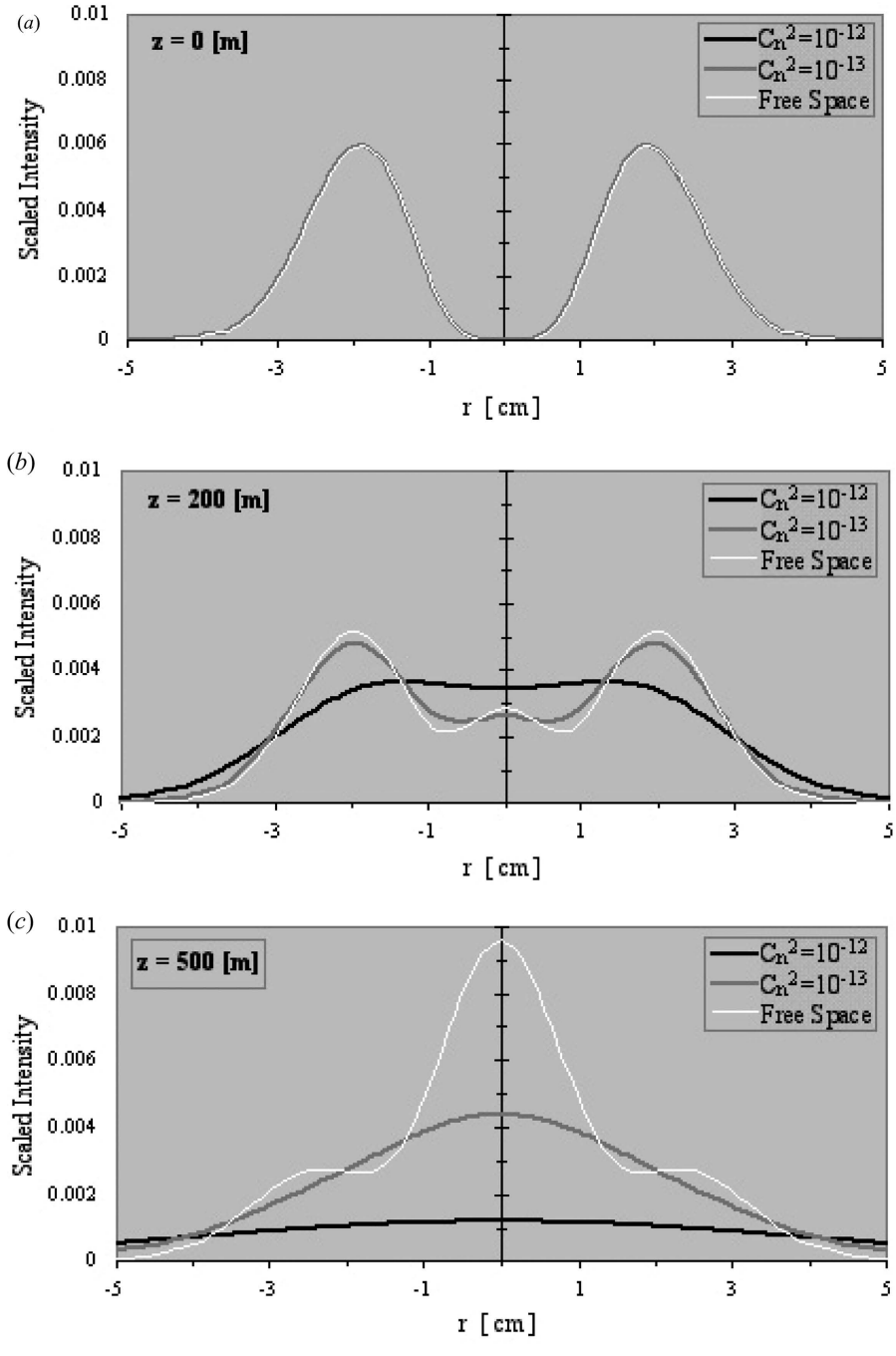

Figure 17.6 Mean irradiance profile of an annular beam (a) at the transmitter, (b) at propagation distance 200 m, and (c) at propagation distance 500 m. The beam radii are 1.8 and 2 cm and the wavelength is $\lambda = 1.55$ μm.

For the annular beam we can express the ratio of free-space optical fields in the form

$$\begin{aligned}\frac{U_0(\mathbf{s},z)}{U_0(\mathbf{r},L)} &= \frac{U_{A,0}(\mathbf{s},z)-U_{B,0}(\mathbf{s},z)}{U_{A,0}(\mathbf{r},L)-U_{B,0}(\mathbf{r},L)} \\ &= \varepsilon_A(\mathbf{r},L)\frac{U_{A,0}(\mathbf{s},z)}{U_{A,0}(\mathbf{r},L)}-\varepsilon_B(\mathbf{r},L)\frac{U_{B,0}(\mathbf{s},z)}{U_{B,0}(\mathbf{r},L)},\end{aligned} \tag{44}$$

where

$$\varepsilon_A(\mathbf{r},L)=\frac{U_{A,0}(\mathbf{r},L)}{U_0(\mathbf{r},L)},\qquad \varepsilon_B(\mathbf{r},L)=\frac{U_{B,0}(\mathbf{r},L)}{U_0(\mathbf{r},L)}. \tag{45}$$

Note that $\varepsilon_A(\mathbf{r},L)-\varepsilon_B(\mathbf{r},L)=1$. Based on (45), it is now convenient to write the first-order complex phase (44) as a difference, viz.,

$$\psi_1(\mathbf{r},L)=\psi_{A,1}(\mathbf{r},L)-\psi_{B,1}(\mathbf{r},L), \tag{46}$$

where

$$\psi_{A,1}(\mathbf{r},L)=\frac{k^2}{2\pi}\varepsilon_A(\mathbf{r},L)\int_0^L dz\int\int_{-\infty}^{\infty}d^2s\exp\left[ik(L-z)+\frac{ik|\mathbf{s}-\mathbf{r}|^2}{2(L-z)}\right]\frac{U_{A,0}(\mathbf{s},z)}{U_{A,0}(\mathbf{r},L)}\frac{n_1(\mathbf{s},z)}{(L-z)}, \tag{47}$$

$$\psi_{B,1}(\mathbf{r},L)=\frac{k^2}{2\pi}\varepsilon_B(\mathbf{r},L)\int_0^L dz\int\int_{-\infty}^{\infty}d^2s\exp\left[ik(L-z)+\frac{ik|\mathbf{s}-\mathbf{r}|^2}{2(L-z)}\right]\frac{U_{B,0}(\mathbf{s},z)}{U_{B,0}(\mathbf{r},L)}\frac{n_1(\mathbf{s},z)}{(L-z)}. \tag{48}$$

In terms of (47) and (48), we note that the scintillation index is defined by

$$\sigma_I^2(\mathbf{r},L)=2\mathrm{Re}[E_2(\mathbf{r},\mathbf{r})+E_3(\mathbf{r},\mathbf{r})], \tag{49}$$

where

$$\begin{aligned}E_2(\mathbf{r},\mathbf{r}) &= E_{AA,2}(\mathbf{r},\mathbf{r})+E_{BB,2}(\mathbf{r},\mathbf{r})-E_{AB,2}(\mathbf{r},\mathbf{r})-E_{BA,2}(\mathbf{r},\mathbf{r}),\\ E_3(\mathbf{r},\mathbf{r}) &= E_{AA,3}(\mathbf{r},\mathbf{r})+E_{BB,3}(\mathbf{r},\mathbf{r})-E_{AB,3}(\mathbf{r},\mathbf{r})-E_{BA,3}(\mathbf{r},\mathbf{r}),\end{aligned} \tag{50}$$

$$\begin{aligned}&E_{AA,2}(\mathbf{r},\mathbf{r})=\langle\psi_{A,1}(\mathbf{r},L)\psi_{A,1}^*(\mathbf{r},L)\rangle, \quad E_{AA,3}(\mathbf{r},\mathbf{r})=\langle\psi_{A,1}(\mathbf{r},L)\psi_{A,1}(\mathbf{r},L)\rangle,\\ &E_{BB,2}(\mathbf{r},\mathbf{r})=\langle\psi_{B,1}(\mathbf{r},L)\psi_{B,1}^*(\mathbf{r},L)\rangle, \quad E_{BB,3}(\mathbf{r},\mathbf{r})=\langle\psi_{B,1}(\mathbf{r},L)\psi_{B,1}(\mathbf{r},L)\rangle,\\ &E_{AB,2}(\mathbf{r},\mathbf{r})=\langle\psi_{A,1}(\mathbf{r},L)\psi_{B,1}^*(\mathbf{r},L)\rangle, \quad E_{AB,3}(\mathbf{r},\mathbf{r})=\langle\psi_{A,1}(\mathbf{r},L)\psi_{B,1}(\mathbf{r},L)\rangle,\\ &E_{BA,2}(\mathbf{r},\mathbf{r})=\langle\psi_{B,1}(\mathbf{r},L)\psi_{A,1}^*(\mathbf{r},L)\rangle, \quad E_{BA,3}(\mathbf{r},\mathbf{r})=\langle\psi_{B,1}(\mathbf{r},L)\psi_{A,1}(\mathbf{r},L)\rangle.\end{aligned} \tag{51}$$

In our analysis, we will confine our expressions to the on-axis ($r=0$) terms only, in which case we write

$$\sigma_I^2(0,L)=\sigma_{I,AA}^2(0,L)+\sigma_{I,BB}^2(0,L)-2\sigma_{I,AB}^2(0,L), \tag{52}$$

where we recognize that $\sigma_{I,AB}^2(0,L)=\sigma_{I,BA}^2(0,L)$. Based on weak irradiance fluctuations and the Kolmogorov spectrum, it follows from results presented

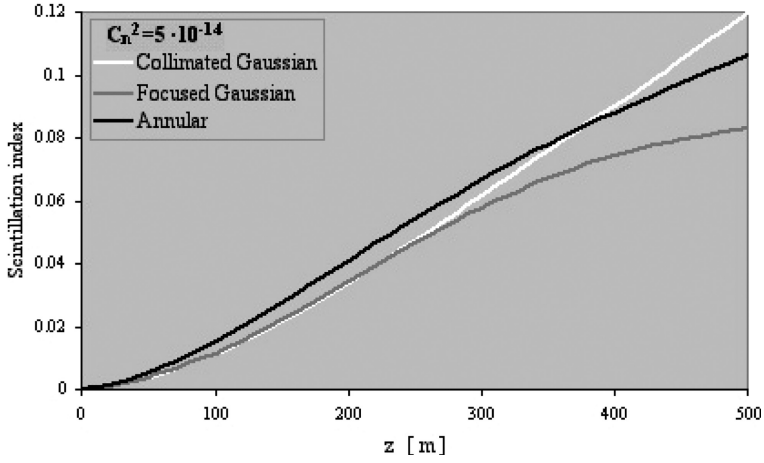

Figure 17.7 The on-axis scintillation index under weak irradiance fluctuations for an annular beam, a collimated beam, and a convergent beam.

in Chap. 8 that

$$\begin{aligned}
&\sigma_{I,AA}^2(0,L)\\
&\quad = 2\mathrm{Re}\left[E_{AA,2}(0,0)+E_{AA,3}(0,0)\right]\\
&\quad = 3.86\sigma_R^2\mathrm{Re}\left[i^{5/6}\frac{U_{A,0}^2(0,L)}{U_0^2(0,L)}\,{}_2F_1\left(-\frac{5}{6},\frac{11}{6};\frac{17}{6};\overline{\Theta}_A+i\Lambda_A\right)-\frac{11}{6}\frac{I_{A,0}(0,L)}{I^0(0,L)}\Lambda_A^{5/6}\right],
\end{aligned} \tag{53}$$

$$\begin{aligned}
&\sigma_{I,BB}^2(0,L)\\
&\quad = 2\mathrm{Re}\left[E_{BB,2}(0,0)+E_{BB,3}(0,0)\right]\\
&\quad = 3.86\sigma_R^2\mathrm{Re}\left[i^{5/6}\frac{U_{B,0}^2(0,L)}{U_0^2(0,L)}\,{}_2F_1\left(-\frac{5}{6},\frac{11}{6};\frac{17}{6};\overline{\Theta}_B+i\Lambda_B\right)-\frac{11}{6}\frac{I_{B,0}(0,L)}{I^0(0,L)}\Lambda_B^{5/6}\right],
\end{aligned} \tag{54}$$

$$\begin{aligned}
&\sigma_{I,AB}^2(0,L)\\
&\quad = \mathrm{Re}\left[E_{AB,2}(0,0)+E_{BA,2}(0,0)+2E_{AB,3}(0,0)\right]\\
&\quad = 3.86\sigma_R^2\mathrm{Re}\left\{i^{5/6}\frac{U_{A,0}(0,L)U_{B,0}(0,L)}{U_0^2(0,L)}\,{}_2F_1\left[-\frac{5}{6},\frac{11}{6};\frac{17}{6};\frac{\overline{\Theta}_A+\overline{\Theta}_B+i(\Lambda_A+\Lambda_B)}{2}\right]\right.\\
&\qquad \left.-\frac{11}{6}\sqrt{\frac{I_{A,0}(0,L)I_{B,0}(0,L)}{I^0(0,L)}}\left(\frac{L}{k}\right)^{5/6}\left(\omega^2+\Delta F^2\right)^{5/12}\cos\left[\frac{5}{6}\tan^{-1}\left(\frac{\Delta F}{\omega}\right)-\Delta\varphi\right]\right\}
\end{aligned} \tag{55}$$

In (55), we have introduced the additional parameter

$$\omega = \frac{1}{W_A} + \frac{1}{W_B}. \tag{56}$$

The on-axis scintillation index of an annular beam is compared with that of a collimated beam equal to beam A and a convergent beam as a function of propagation distance out to 500 m. The index of refraction structure constant is set at $C_n^2 = 5 \times 10^{-14}\ \mathrm{m}^{-2/3}$, the inner scale is zero, and the outer scale is infinite. Once again we set the beam radii of the annular beam to 1.8 and 2 cm and wavelength to 1.55 μm. The convergent beam has the same size at the transmitter as the collimated beam and is assumed focused at 1000 m. Although the annular beam shows a higher scintillation level over the first part of the path, its scintillation level is lower than the collimated beam after 400 m and will remain so over a long distance. The convergent beam (neglecting effects of beam wander) has an on-axis scintillation index that is still lower than the annular beam.

17.4 Other Beams

In addition to the beam shapes discussed thus far, there are several others that have appeared in the literature over the years but their propagation behavior in optical turbulence has not been examined to the best of our knowledge. We briefly discuss some of these below in terms of their free-space properties.

17.4.1 Flattened Gaussian profiles

In some applications it can be important for the field amplitude (irradiance) of the optical wave to be as uniform as possible in the center portion of the beam with a sharp falloff outside this area [9]. Such an optical wave is similar to a "top-hat" beam but without the ringing phenomenon such as that associated with a uniform plane wave incident on a circular aperture. One of the most popular examples of this kind of optical wave is provided by the class of *super-Gaussian* (SG) profiles that have the functional form in the plane of the transmitter aperture given by [10,11]

$$U_0(\mathbf{r}, 0) = A_0 \exp\left[-\left(\frac{r}{W_0}\right)^{\gamma}\right], \tag{57}$$

where A_0 is the maximum amplitude. For $\gamma = 2$ we obtain the conventional Gaussian TEM_{00} wave and in the limit $\gamma \to \infty$ it approaches a top-hat or axially-symmetric rectangle function. Because it is not very tractable for general γ, even the study of free-space propagation features of (57) is usually done numerically.

To overcome the numerical difficulties associated with the super-Gaussian profile (57), other related models have been proposed. Of particular interest in this regard is the so-called flattened Gaussian (FG) profile which can be studied

through use of the paraxial equation [12–14]. The analytical representation of this class of flattened beams in one dimension is

$$U_0(x,0;N) = A_0 \exp\left[-\frac{(N+1)x^2}{W_{x,0}^2}\right] \sum_{n=0}^{N} \frac{1}{n!}\left[\frac{(N+1)x^2}{W_{x,0}^2}\right]^n, \tag{58}$$

where $W_{x,0}$ is the width of the profile and N is the order of the FG profile related to its flatness. For $N = 0$ the FG profile reduces to the standard Gaussian beam and in the limit $N \to \infty$ it tends to a top hat (or rectangle) like in the case of a SG profile. One advantage offered by the FG beam is that it is directly related to the Hermite-Gaussian modes in a rectangular geometry and is related to the Laguerre-Gaussian modes in the axially symmetric case. To see this, we first note that for the Laguerre-Gaussian modes we have

$$x^n = n! \sum_{k=0}^{n} \binom{n}{k} (-1)^k L_k(x). \tag{59}$$

Consequently, using (58) and (59) we can write the axially symmetric FG profile in terms of the Laguerre polynomials according to

$$\begin{aligned} U_0(r,0;N) &= A_0 \exp\left[-\frac{(N+1)r^2}{W_0^2}\right] \sum_{n=0}^{N} \frac{1}{n!}\left[\frac{(N+1)r^2}{W_0^2}\right]^n \\ &= A_0 \exp\left[-\frac{(N+1)r^2}{W_0^2}\right] \sum_{n=0}^{N} \sum_{k=0}^{n} \binom{n}{k} \frac{(-1)^k}{2^n} L_k\left[\frac{2(N+1)r^2}{W_0^2}\right]. \end{aligned} \tag{60}$$

Based on (60) for the FG beam at the transmitter, the corresponding FG beam at distance L from the transmitter can be obtained from the Huygens-Fresnel integral for free space, which yields

$$\begin{aligned} U_0(r,L;N) = A_0 \frac{W_N(0)}{W_N(L)} &\exp\left[ikL - i\Phi_N(L) - \frac{r^2}{W_N^2(L)} - \frac{ikr^2}{2F_N(L)}\right] \\ &\times \sum_{n=0}^{N} \sum_{k=0}^{n} \binom{n}{k} \frac{(-1)^k}{2^n} L_k\left[\frac{2r^2}{W_N^2(L)}\right] \exp[-2in\Phi_N(L)], \end{aligned} \tag{61}$$

where

$$W_N(0) = \frac{W_0}{\sqrt{N+1}}, \tag{62}$$

$$W_N(L) = W_N(0)\sqrt{1 + \left[\frac{2L}{kW_N^2(0)}\right]^2} = W_0\sqrt{\frac{1}{N+1} + (N+1)\Lambda_0^2}, \tag{63}$$

$$F_N(L) = -L\left\{1 + \left[\frac{kW_N^2(0)}{2L}\right]^2\right\} = -\frac{kW_0^2}{2(N+1)}\left[\frac{1 + (N+1)^2\Lambda_0^2}{(N+1)\Lambda_0}\right], \tag{64}$$

$$\varphi_N(L) = \tan^{-1}[(N+1)\Lambda_0]. \tag{65}$$

Clearly, for $N = 0$ the above results (60)–(65) reduce to those associated with the TEM_{00} Gaussian-beam wave. Similar results can be deduced for the Hermite-Gaussian modes by simply recognizing that

$$x^{2m} = \frac{(2m)!}{2^{2m}} \sum_{k=0}^{m} \frac{H_{2k}(x)}{(2k)!(m-k)!},$$
$$x^{2m+1} = \frac{(2m+1)!}{2^{2m-1}} \sum_{k=0}^{m} \frac{H_{2k+1}(x)}{(2k+1)!(m-k)!}. \tag{66}$$

Although the above one-dimensional FG beam (58) becomes more and more flattened as N increases (approaching a rectangular shape), this is not the case as the beam propagates. In fact, it can be shown that the more flattened the beam appears in the plane of the transmitter (i.e., the waist plane), the more distorted it becomes as it propagates. In particular, in the limit $N \to \infty$ it has been shown that the on-axis intensity approaches the function [13]

$$I_\infty(0, L) = 4|A_0|^2 \sin^2\left(\frac{1}{2\Lambda_0}\right), \tag{67}$$

corresponding to the on-axis intensity for a circular aperture.

17.4.2 Family of Bessel beams

In recent years there has been a lot of interest in the propagation of diffraction-free beams at optical frequencies [15–19]. Among these are the Bessel beam [15,16], the Bessel-Gauss beam [17], and the azimuthal Bessel-Gauss (ABG) beam [18,19].

Durnin [15] presented the first free-space, beamlike, exact solutions of the wave equation that are diffraction-free after the plane where the beam is formed. Like the infinite plane wave, however, such solutions have finite energy density rather than finite energy. By nondiffracting we mean its transverse distribution does not change as it propagates. In the simplest type of nondiffracting beam which is circularly symmetric the transverse disturbance distribution has the form of a Bessel function of the first kind and order zero—hence, the name *Bessel beam*. The optical field of this beam at distance L from the transmitter plane takes the simple form

$$U_0(r, L) = A_0 e^{i\beta L} J_0(\alpha r), \tag{68}$$

where A_0 is a constant amplitude and $\beta^2 + \alpha^2 = k^2$. When $\alpha = 0$, the solution (68) is simply that of a plane wave, but for $0 < \alpha \leq k$ the solution is a nondiffracting beam whose intensity profile decays at a rate proportional to $1/\alpha r$.

If we consider the limiting case of the Bessel beam to reduce to a Gaussian function rather than an infinite plane wave, then the optical wave field can be

represented at the exit aperture of a transmitter by

$$U_0(r,0) = AJ_0(\alpha r)\exp\left(-\frac{r^2}{W_0^2}\right), \tag{69}$$

where A is an amplitude factor (possibly complex) and W_0 is the radius of the Gaussian term. For obvious reasons, such a beam is called a *Bessel-Gauss beam*. Gori et al. [17] have shown that the field of the Bessel-Gauss beam (69) at distance L from the transmitter can be expressed as

$$\begin{aligned} U_0(r,L) = \frac{AW_0}{W(L)}\exp\left[i\left(k-\frac{\alpha^2}{2K}\right)L - i\varphi(L)\right]J_0\left(\frac{\alpha r}{1+\Lambda_0}\right) \\ \times \exp\left(-\frac{r^2}{W^2(L)} - \frac{ikr^2}{2F(L)}\right)\exp\left(-\frac{\alpha^2L^2}{k^2W^2(L)} - \frac{ik\alpha^2L^2}{2kF(L)}\right), \end{aligned} \tag{70}$$

where

$$W(L) = W_0\sqrt{1+\Lambda_0^2}, \tag{71}$$

$$F(L) = -\frac{kW_0^2}{2}\left(\frac{1+\Lambda_0^2}{\Lambda_0}\right), \tag{72}$$

$$\varphi(L) = \tan^{-1}\Lambda_0. \tag{73}$$

Note that (71)–(73) are the same expressions that occur in the propagation of a collimated TEM_{00} Gaussian beam (see Chap. 4). In fact, for $\alpha = 0$ Eq. (70) reduces to that of the Gaussian-beam wave.

Jordan and Hall [18] and Greene and Hall [19] have likewise examined diffraction characteristics of the *azimuthal Bessel-Gauss beam*. The term azimuthal polarization refers to the field in cylindrical coordinates (r,θ,z) propagating along the positive z-axis with the electric field everywhere directed along the unit vector $\hat{\theta}$ in the azimuthal direction. The scalar field in this case possesses a distinct axial null in both the near- and far-field radiation patterns that is characterized at the exit aperture of the transmitter by

$$U_0(r,0) = AJ_1(\alpha r)\exp\left(-\frac{r^2}{W_0^2}\right), \tag{74}$$

which differs from (69) only by the order of the Bessel function. Similar to (70), the scalar field at propagation distance L becomes

$$\begin{aligned} U_0(r,L) = \frac{AW_0}{W(L)}\exp\left[i\left(k-\frac{\alpha^2}{2k}\right)L - i\varphi(L)\right]J_1\left(\frac{\alpha r}{1+\Lambda_0}\right) \\ \times \exp\left(-\frac{r^2}{W^2(L)} - \frac{ikr^2}{2F(L)}\right)\exp\left(-\frac{\alpha^2L^2}{k^2W^2(L)} - \frac{ik\alpha^2L^2}{2kF(L)}\right), \end{aligned} \tag{75}$$

where the parameters are the same as (71)–(73).

17.5 Summary and Discussion

The analysis of optical wave propagation through random media other than plane waves, spherical waves, and the lowest-order TEM_{00} Gaussian-beam wave is quite sparse in the literature. In this chapter we have briefly examined the higher-order Hermite-Gaussian modes and higher-order Laguerre-Gaussian modes and found that the relative beam spreading of these higher-order modes in optical turbulence is less than that of a lowest-order Gaussian beam. A similar result was also obtained in the case of an annular beam. The exploitation of these results in particular optical systems has not yet been done to the authors' knowledge.

Of particular significance is the fact that the on-axis scintillation index of an annular beam is lower than that of a corresponding Gaussian beam of similar aperture size at the transmitter. Off-axis irradiance fluctuations have not been analyzed but it is presumed that off-axis fluctuations may be stronger than the corresponding fluctuations of a collimated Gaussian beam. If so, this means that accurate pointing will be necessary to take advantage of the lower on-axis scintillation level in a FSO communication system or other application where scintillation is of great concern.

Problems

Section 17.2

1. Show that substitution of the mean irradiance

$$\langle I_{10}(x,y,z)\rangle_y = \frac{W_0}{W\sqrt{1+1.78\Lambda\sigma_R^2}}\exp\left[-\frac{2y^2}{W^2\left(1+1.78\Lambda_R^2\right)}\right]$$

into (4) leads to

$$\sigma_{y,0,\mathrm{LT}} = W\sqrt{1+1.78\Lambda\sigma_R^2}.$$

2. Show that substitution of the mean irradiance

$$\langle I_{10}(x,y,z)\rangle_x = \frac{W_0}{W\sqrt{1+1.78\Lambda\sigma_R^2}}\left[\frac{8x^2}{W^2\left(1+1.78\Lambda\sigma_R^2\right)^2}+\frac{3.56\Lambda_0\sigma_R^2(1+\Lambda\sigma_R^2)}{\left(1+1.78\Lambda\sigma_R^2\right)^2}\right] \times \exp\left[-\frac{2x^2}{W^2\left(1+1.78\Lambda\sigma_R^2\right)}\right]$$

into (4) leads to

$$\sigma_{x,1,\mathrm{LT}} = W\sqrt{1+1.78\Lambda\sigma_R^2}\sqrt{\frac{3(1+1.78\Lambda\sigma_R^2)+1.78\Lambda_0\sigma_R^2(1+\Lambda\sigma_R^2)}{1+1.78\Lambda\sigma_R^2+1.78\Lambda_0\sigma_R^2(1+\Lambda\sigma_R^2)}}.$$

3. Given the expression [see (38) in Chap. 6]

$$T = 4\pi^2k^2z\int_0^1\int_0^\infty \kappa\Phi_n(\kappa)\left(1-e^{-\Lambda z\kappa^2\xi^2/k}\right)d\kappa d\xi,$$

use the geometrical optics approximation

$$1-e^{-\Lambda z\kappa^2\xi^2/k} \cong \frac{\Lambda z\kappa^2\xi^2}{k}, \qquad \frac{z\kappa^2}{k} \ll 1,$$

to show that

$$W^2T = \frac{8}{3}\pi^2z^3\int_0^\infty \kappa^3\Phi_n(\kappa)d\kappa.$$

4. Define $s = 0.89\sigma_R^2$ and show that the mean irradiance

$$\langle I_{10}(r,\theta,z)\rangle = \left(A+\frac{Br^2}{W^2}+\frac{Cr^4}{W^4}\right)\exp\left[-\frac{2r^2}{W^2(1+1.78\Lambda\sigma_R^2)}\right]$$

(*a*) substituted into (20) leads directly to

$$\sigma_{0,1,\mathrm{LT}}^2 = W^2(1+2\Lambda s)\left\{\frac{2A+(1+2\Lambda s)[2B+3C(1+2\Lambda s)]}{A+(1+2\Lambda s)[B+C(1+2\Lambda s)]}\right\}.$$

(*b*) On simplification of the result in part (*a*), deduce that [see (24) and (25)]

$$\sigma^2_{0,1,\mathrm{LT}} = W^2(3 + 2\Lambda s) = W^2(3 + 1.78\Lambda\sigma_R^2).$$

Section 17.3

5. In the absence of atmospheric turbulence (i.e., $C_n^2 = 0$), show that the mean irradiance (42) reduces to an expression equivalent to (32).
6. Show that the far-field irradiance of a plane wave incident on a "hard" annular aperture $0 < a < r < b$ leads to an expression that is proportional to (neglect atmospheric turbulence)

$$I \sim \left| \frac{bJ_1(b\rho) - aJ_1(a\rho)}{\rho} \right|^2.$$

References

1. H. W. Kogelnik and T. Li, "Laser beams and resonators," *Appl. Opt.* **5**, 1550–1567 (1966).
2. A. Siegman, *Lasers* (University Science, Mill Valley, Calif., 1986).
3. W. H. Carter, "Spot size and divergence for Hermite Gaussian beams of any order", *Appl. Opt.* **19**, 1027–1029 (1980); "Energy carried over the rectangular spot within a Hermite-Gaussian beam," *Appl. Opt.* **21**, 7 (1982).
4. R. L. Phillips and L. C. Andrews, "Spot size and divergence for Laguerre Gaussian beams of any order," *Appl. Opt.* **22**, 643–644 (1983).
5. C. Y. Young, Y. V. Gilchrist, and B. R. Macon, "Turbulence induced beam spreading of higher order mode optical waves," *Opt. Eng.* **41**, 1097–1103 (2002).
6. T. Shirai, A. Dogariu, and E. Wolf, "Mode analysis of spreading of partially coherent beams propagating through atmospheric turbulence," *J. Opt. Soc. Am. A* **20**, 1094–1102 (2003).
7. M. Born and E. Wolf, *Principles of Optics*, 7th ed. (Cambridge University Press, Cambridge, 2002).
8. F. E. Strömqvist Vetelino and L. C. Andrews, "Annular Gaussian beams in turbulent media," *Proc. SPIE* **5160**, 86–97 (2003).
9. C. S. Ih, "Absorption lens for producing uniform laser beams," *Appl. Opt.* **11**, 694–697 (1972).
10. S. De Silvestri, P. Laporta, V. Magni, and O. Svelto, "Solid-state laser unstable resonators with tapered reflectivity mirrors: the super-Gaussian approach," *IEEE J. Quantum Electron.* **24**, 1172–1177 (1988).
11. A. Parent, M. Morin, and P. Lavigne, "Propagation of super-Gaussian field distributions," *Opt. Quantum Electron.* **24**, 1071–1079 (1992).
12. F. Gori, "Flattened Gaussian beams," *Opt. Commun.* **107**, 335–341 (1994).
13. V. Bagini, R. Borghi, F. Gori, A. M. Pacileo, M. Santarsiero, D. Ambrosini, and G. Schirripa Spagnolo, "Propagation of axially symmetric flattened Gaussian beams," *J. Opt. Soc. Am. A* **13**, 1385–1394 (1996).
14. M. Santarsiero and R. Borghi, "Correspondence between super-Gaussian and flattened Gaussian beams," *J. Opt. Soc. Am.* **16**, 188–190 (1999).
15. J. Durnin, "Exact solutions for nondiffracting beams. I. The scalar theory," *J. Opt. Soc. Am. A* **4**, 651–654 (1987).
16. J. Durnin, J. J. Micelli, and J. H. Eberly, "Diffraction-free beams," *Phys. Rev. Lett.* **58**, 1499–1501 (1987).
17. F. Gori, G. Guattari, and C. Padovani, "Bessel-Gauss beams," *Opt. Commun.* **64**, 491–495 (1987).
18. R. H. Jordan and D. G. Hall, "Free-space azimuthal paraxial wave equation: the azimuthal Bessel-Gauss beam solution," *Opt. Lett.* **19**, 427–429 (1994).
19. P. L. Greene and D. G. Hall, "Diffraction characteristics of the azimuthal Bessel-Gauss beam," *J. Opt. Soc. Am. A* **13**, 962–966 (1996).